Spectral Transmittance of Lossy Printed Resonant-Grid Terahertz Bandpass Filters

Michael E. MacDonald, *Member, IEEE*, Angelos Alexanian, Robert A. York, *Senior Member, IEEE*, Zoya Popović, *Senior Member, IEEE*, and Erich N. Grossman

***Abstract*—In this paper, we present terahertz bandpass filters composed of resonant arrays of crossed slots in lossy metal films deposited on dielectric membranes. The filters exhibit insertion loss as low as 1.9 dB at room temperature and 1.2 dB at 77 K at a center frequency of 2.2 THz. It is found that the dielectric substrate introduces a downward shift in frequency not predicted by standard mean dielectric-constant approximations. This shift is proportional to the permittivity and thickness of the substrate, and is accurately modeled for polyester, fused quartz and silicon substrates using a finite-difference time-domain (FDTD) model. It is also found that the insertion loss and Q-factors of the filters vary with the product of the thickness and conductivity of the metal film for lead and gold films, even in cases when the thickness is several skin depths at the center frequency. The FDTD theory presented here accounts for some of the conductor losses.**

***Index Terms*—FSS, spatial filters, terahertz.**

I. Introduction

TERAHERTZ receivers require filtering elements to reject thermal radiation that may otherwise saturate sensitive detectors. The architecture of quasi-optical receiver systems suggests the use of frequency-selective surfaces (FSS's) [1] as filtering elements. These surfaces are periodic arrays of strip (dipole) or slot elements, which behave as bandstop and bandpass filters, respectively. Several such grid geometries have been demonstrated, including arrays of annular and square rings, dipoles, tripoles, crosses, and Jerusalem crosses (a good overview is presented in [1]). Another example of a bandpass filter is a grid of crossed resonant slots [2], [3]. These filters may be printed on substrates, or electroplated as freestanding grids for reduced loss in the passband [4], [5]. Substrate-supported FSS's are of interest since they are much easier to fabricate and can have reasonably low loss, which can further be reduced if they are mounted on a cold stage used for cryogenic detectors. It has also been shown that for systems that have focused beams with low f numbers, in which case the waves do not have an equiphase wavefront, the shifts in resonant frequency due to oblique incident angles can be reduced by the substrate [6].

The filters presented here are fabricated by evaporating thin gold or lead films on electrically thin polyester (Mylar) substrates. Lead and gold have been chosen since their bulk conductivities differ significantly. The thickness of evaporated gold and lead films was varied from 20 nm to 1 μm, and 100 nm to 1.4 μm, respectively, in order to vary the conductor losses over a wide range. The passband insertion loss and Q-factor of all filters was found to vary with the dc surface resistance R_S of the metal film, over nearly three orders of magnitude in R_S. This result is surprising because the metal films are several skin depths thick over most of the range of values of R_S investigated here. The stopband attenuation was found to vary only weakly with R_S, and only for the films that were not much thicker than the skin depth. The differences in variation between the passband and stopband attenuation are probably due to the resonant nature of the filters, as well as the sensitivity of the passband loss to microstructural effects present in thin evaporated films. Comparison with published results for electroplated freestanding filters [4], [5] indicate that thick metal films with bulk-like properties appear to be necessary in order to achieve less than 1-dB insertion loss.

The substrate causes a downward shift in resonant frequency, which is larger for thicker substrates. This shift in frequency reaches a limiting value scaled by the square root of the mean permittivity when the substrate is roughly a tenth of the free-space resonant wavelength thick. A finite-difference time-domain (FDTD) model [7] has been extended in this paper to incorporate conductor losses. The model accurately predicts the measured frequency shift, and also predicts a portion of the transmission loss. The difference between the predictions and measurements are discussed in Section V.

We conclude that the simple fabrication of the filters and their reasonable performance makes them useful elements at far-infrared wavelengths, despite the added loss as compared to freestanding FSS's.

II. Geometry and Modeling of Grid Filters

The grid geometry and unit cell investigated in this paper are shown in Fig. 1. The geometry is defined by the slot length L, the slot width W, and the period P. The slot dimensions determine the frequency response of the filter, as shown in [8]. The width of the slot controls the shape of the resonant frequency response and, thus, the Q-factor (where $Q = f_0/(2\Delta f)$ and Δf is the 3-dB bandwidth). In [8], an empirical formula is given for

Manuscript received March 5, 1999; revised September 13, 1999. This work was supported by the Army Research Office under the Multidisciplinary Research Initiative Grant DAAH04-98-1-0001, by the NASA Office of Space Sciences, and under the Cooperative Research and Development Agreement with Idaho National Engineering Laboratories.

M. E. MacDonald and E. N. Grossman are with the National Institute of Standards and Technology, Boulder, CO 80303 USA.

A. Alexanian and R. A. York are with the Department of Electrical and Computer Engineering, University of California at Santa Barbara, Santa Barbara, CA 93106 USA.

Z. Popović is with the Department of Electrical and Computer Engineering, University of Colorado at Boulder, Boulder, CO 80309 USA.

Publisher Item Identifier S 0018-9480(00)02530-8.

0018–9480/00$10.00 © 2000 IEEE

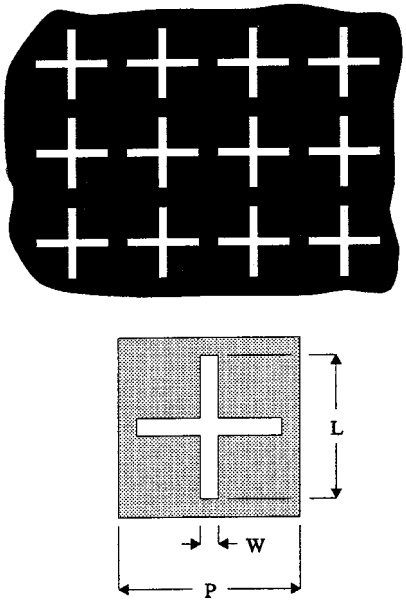

Fig. 1. Grid filter geometry and square unit cell of the grid.

the resonant wavelength for grids where $W/(P-L) < 1$ as follows:

$$\lambda_0 = 2.1L. \tag{1}$$

The grid period determines the wavelength at which diffraction causes grating lobes. The longest wavelength (lowest frequency) at which diffraction occurs for a given incidence angle θ_i is $\lambda_D = P(1+\sin\theta_i)$. Since the period is larger than the slot length, λ_D approaches λ_0 for large angles of incidence, which affects the shape of the passband. Diffraction obviously becomes a concern when two or more grids are cascaded [2].

The filters presented in this paper were modeled using a FDTD technique that employs Floquet boundary conditions for normal incidence, so that the problem of analyzing an infinite grid is reduced to that of a single-unit cell. The effect of the dielectric substrate can be accurately modeled by this technique, as demonstrated in Section III. The studies of conductor losses, discussed in Section IV, required the extension of the FDTD model [7]. The conductivity of the metal film is taken into account in the discretized wave equations and the surface impedance is determined at the resonant frequency under the assumption that the film thickness is larger than the skin depth.

III. Filter Fabrication and Characterization

The filters are fabricated on 3.8-μm-thick polyester substrates using standard photolithographic equipment. The substrates are glued with photoresist to the perimeter of a 7.5-cm (3-in) carrier silicon wafer. In the fabrication process, the polyester is heated to 110 °C to stretch flat on the wafer. In this way, a polyester "drum skin," supported at its edges, is formed. A small hole is cut in the polyester to avoid air trapping under the dielectric membrane, which would have caused focusing problems due to the small depth of field of the stepper camera used in the photolithographic process. The membrane is then coated with photoresist and soft baked at 95 °C. After exposure and development, the wafers are loaded into a vacuum system and a 10-min sputter cleaning is performed in a 1.33-Pa (10^{-2} torr) argon plasma to promote adhesion of the gold or lead metal film. After evaporation and liftoff, a second longer acetone soak dissolves the resist that holds the filter to the carrier wafer. The filter and carrier are then moved to a spinner while still flooded with acetone, and the acetone is carefully drained off the wafer until the filter clings to the wafer. As the remaining acetone is spun off, the filter flattens on the wafer. An aluminum ring is then glued to the filter, and the filter is then peeled off from the carrier wafer. The process described above results in an optically flat grid on a rigid carrier ring.

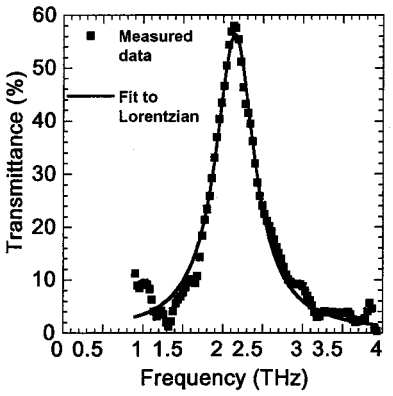

Fig. 2. Measured transmittance as a function of frequency. The solid line shows a fit to the Lorentzian shape given by (2).

The spectral transmittance of the filters is measured in a commercial Fourier-transform spectrometer (FTS). The portion of the FTS that contains the source, i.e., interferometer and detector, is sealed and desiccated. The sample chamber is continuously purged with dry nitrogen to minimize errors due to atmospheric absorption. Measurements of filter spectra are calibrated by background spectra taken through the empty chamber immediately beforehand.

The development of the filters presented here was motivated by the need to reject background thermal radiation in order to avoid saturating superconducting mixers. The filters are intended to pass 2.5-THz radiation with as low loss as possible. The period of the grid used here is 70 μm, with slot dimensions $L = 56$ μm and $W = 7$ μm. These dimensions give a resonant frequency of 2.55 THz for a freestanding grid (air substrate). Spectra were measured at normal incidence up to 30 THz with a resolution of 120 GHz, which resulted in good signal-to-noise ratios without broadening any real features of the filter spectrum. The signal-to-noise ratio degrades rapidly at frequencies below 750 GHz due to the Rayleigh–Jeans rolloff of the blackbody radiation. An example of a measured transmittance spectrum is shown in Fig. 2, indicating a Lorentzian shape given by

$$T(f) = \frac{k\alpha}{(f-f_0)^2+\alpha^2} \tag{2}$$

where f_0 is the resonant frequency, α is the half-power width of the resonance profile, and k is a constant. The filters can be characterized by their peak transmittance, resonant frequency,

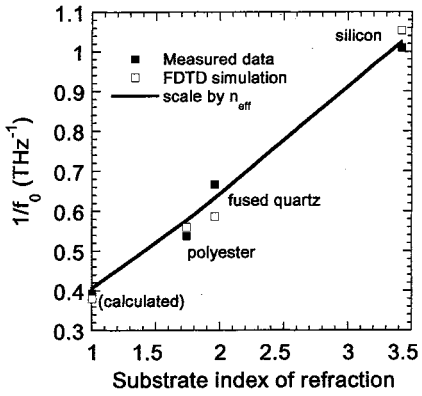

Fig. 3. Reciprocal of the resonant frequency for geometrically identical grids versus the substrate index (permittivity) for substrates 3.8-μm thick. The plot shows that scaling with the effective index from (3) is valid.

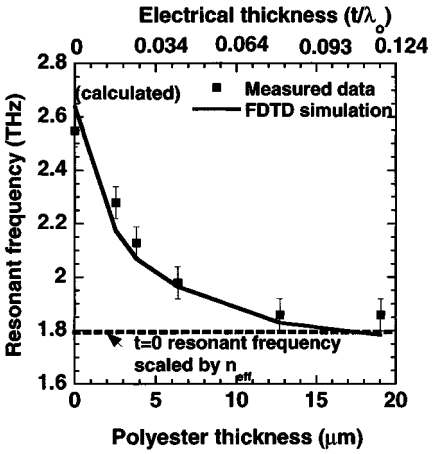

Fig. 4. Resonant frequency of geometrically identical grids versus polyester substrate thickness. The solid line shows FDTD theoretical results [7]. The resonant frequency is affected even by electrically very thin films.

and Q-factor by fitting a curve, as given by (2), to the measured spectra.

The resonant frequency of the substrate-supported grids are shifted downward from the free-space value [9], as shown in Figs. 3 and 4. The shift is a function of permittivity and thickness of the substrate, and is a result of evanescent modes in the substrate [10]. The quasi-static thick-substrate approximation [11] indicates scaling of the resonant frequency inversely with effective index

$$n_{\text{eff}} = \sqrt{\frac{n^2_{\text{substrate}} + 1}{2}}. \tag{3}$$

In Fig. 3, the reciprocal of the resonant frequency is plotted, so that this scaling factor appears as a line. Measurements were performed on thick polyester, quartz, and silicon substrates, and indicate good agreement with (3). Fig. 4 shows the resonant frequency as a function of thickness of polyester substrate, and is compared to the freestanding case as calculated from (1). The measurements illustrate that even the electrically thinnest films cause an appreciable shift in resonant frequency. When the substrate becomes approximately $\lambda_0/10$ thick, the resonant frequency converges to the asymptotic value obtained with use

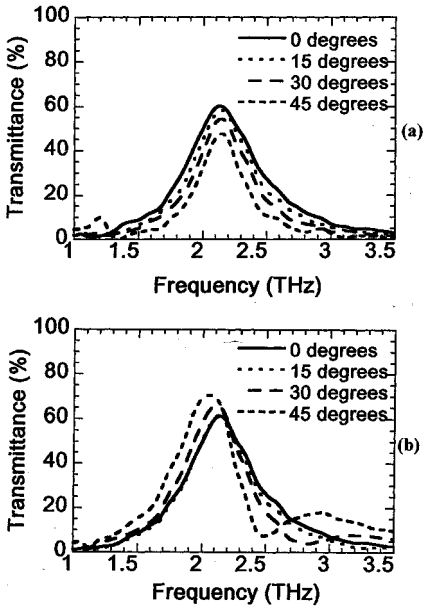

Fig. 5. Measured filter spectra for different angles of oblique incidence for the (a) TE and (b) TM polarization of the incident wave. These measurements were made on a grid filter fabricated on a 3.8-μm polyester substrate with $L = 56$ μm, $W = 7$ μm, and with a period $P = 70$ μm.

of (3). It is seen that the FDTD simulation predicts the resonant frequency within the accuracy of the measurement.

For applications that require that the filter be placed in a focused beam, it is important to know its behavior for angles of incidence other than normal. The spectral transmittance at oblique incidence was measured by inserting a wire polarizer in the FTS to set the incident polarization (TE or TM) and inserting the filter in a rotatable mount. Fig. 5 shows that, in the TM case, there is a null in transmittance (Wood's anomaly), which is due to surface waves along the plane of the grid [6] and occurs at the onset of diffraction. The shapes of the TM spectra agree well with simulations of slot grids of similar geometry [12]. For the TE case, results presented in [12] also show a very narrow-band Wood's anomaly, and we suspect that we do not see it in our measurements because of the course spectral resolution of 120 GHz. The transmittance null associated with Wood's anomaly undergoes a shift in frequency for a substrate-supported grid [6], similar to that of the resonant frequency. For grids fabricated on 3.8-μm polyester substrates, the wavelength of the Wood's anomaly null in the TM case is in good agreement with the $\lambda_D = P(1+\sin\theta_i)$ dependence. Grids fabricated on 12.7-μm-thick substrates show that the frequency of this null is about 8% lower than the value given by the above formula.

IV. Effects of Finite Metal Conductivity on Insertion Loss and Q-Factor

The filters from Fig. 1 show an appreciable insertion loss of 40% at resonance. We have found that this loss varies with the dc surface resistance R_S of the film. The surface resistance is experimentally obtained from four-point probe measurements [13]. The test structure is a 1-cm square of metal fabricated on

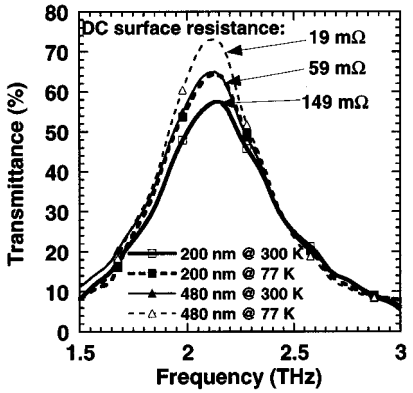

Fig. 6. Measured transmittance of two filters with different gold thicknesses (200 and 480 nm) at 300 and 77 K.

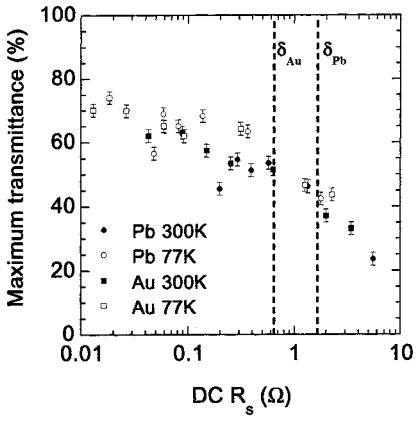

Fig. 7. Peak transmittance of gold and lead films at 300 and 77 K versus the measured dc surface resistance. The vertical lines show the value of R_S calculated for a film that is one skin depth thick for the two metals.

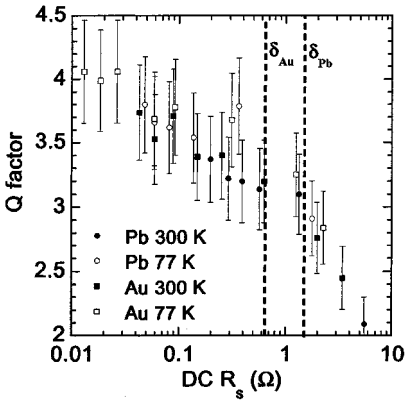

Fig. 8. Q-factor versus the dc surface resistance shows a variation similar to that observed for the insertion loss.

the same wafer as the grid filter and electrically isolated from the grid.

The following three methods were used to vary the dc surface resistance of the film:

1) varying the metal thickness;
2) using two different metals (gold and lead);
3) varying the temperature (300 and 77 K).

In the latter case, the surface resistance was measured by submerging the probes and test structure in liquid nitrogen. Measurements with the FTS at 77 K were obtained by mounting the filter in a small evacuated chamber with polyester windows at each end. The fixture allowed liquid nitrogen to circulate through a copper block, which served as the heat sink for the filter.

The measured spectral transmittance versus surface resistance is shown in Fig. 6. For these measurements, two filters were fabricated using gold films of different thicknesses, and characterized at both 300 and 77 K. The thicknesses are chosen so that the dc surface resistance of the 200-nm—thick film at 77 K is equal to that of the 480-nm-thick film at 300 K. No substantial difference is seen in these two spectra, and this demonstrates that the transmittance varies with conductivity and thickness only through their product, which is the dc surface conductance $(1/R_S)$. This result is somewhat surprising because the films are considerably thicker than a skin depth δ ($\delta = \sqrt{2/(\omega\mu\sigma)}$) and, therefore, the ac surface resistance should be independent of film thickness. At 2.5 THz, $\delta = 55$ nm for gold, calculated by using the measured 300-K dc conductivity of 3.36×10^7 S/m. The general expression for surface impedance as a function of thickness t is

$$Z_S = \sqrt{\frac{\mathrm{j}\omega\mu}{\sigma}}\coth\left(t\sqrt{\mathrm{j}\omega\mu\sigma}\right) \tag{4}$$

which reduces to the dc limit $Z_S = 1/(\delta t)$ for $t \ll \delta$. In the limit when $t \gg \delta$, (4) reduces to the familiar formula $Z_S = (1+\mathrm{j})/(\delta\sigma)$, which is a function only of temperature (through conductivity), and not of thickness [14].

The results of experiments on a large number of filters are summarized in Fig. 7, which shows the peak transmittance plotted versus surface resistance. These measurements show that the four sets of data (gold and lead films at 300 and 77 K) all follow the same trend with respect to the dc surface resistance. The vertical lines on the plot correspond to the dc surface resistance. Although the slope of a line drawn through the data points does appear to decrease when the film thickness becomes greater than a skin depth, it does not decrease to zero. Freestanding grid filters consisting of 12-μm-thick films of electroplated copper have been reported to have negligible loss [5]. The calculated dc surface resistance is 0.0014 Ω for these films, which is approximately one order of magnitude smaller than our lowest R_S. Even if our data is extrapolated to that value, we would expect approximately 80%–85% transmittance, which is much lower than quoted in [5]. One reason for the discrepancy is that the substrate causes losses due to reflection and absorption. Measurements of polyester substrates with no metallization indicate that approximately 7% of the loss in Fig. 7 is due to the substrate, mostly lost to the reflected wave. Fig. 8 shows the variation of the Q-factor with R_S, which also does not seem to agree with the value in [5] of $Q = 7$.

The stopband attenuation of the filters versus R_S is summarized in Fig. 9. The gold film reaches its limiting value at 56 nm, which corresponds to the calculated skin depth at 2.5 THz using the measured conductivity at 300 K. The lead film reaches its limiting value at 182 nm, approximately equal to the 147-nm

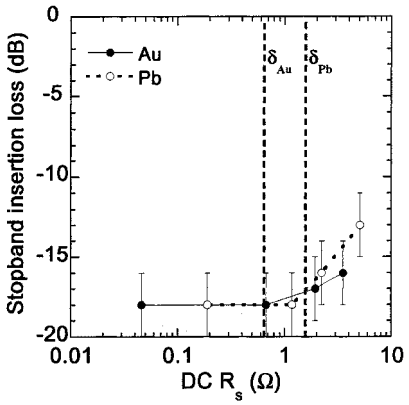

Fig. 9. Stopband attenuation versus the dc surface resistance for gold and lead filters at room temperature. The vertical lines correspond to the skin depths.

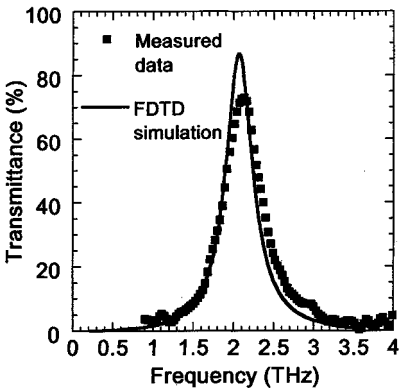

Fig. 10. Measured transmittance versus frequency (symbols) for a gold film as compared to an FDTD simulation that includes bulk metal conductivity (solid line).

skin depth calculated at 2.5 THz using a measured dc conductivity of 0.47×10^7 S/m at 300 K.

The FDTD analysis incorporates conductor losses, but since the assumption must be made that the surface impedance is constant for $t \gg \delta$, the variation in the resonant properties of the filter cannot be accounted for by this method. The spectral transmittance predicted for a gold filter (using the bulk conductivity of 4.6×10^7S/m) by the FDTD model is shown in Fig. 10 along with the gold filter with the highest transmittance. The shape of the spectrum is predicted within approximately 5% of the center frequency. The predicted filter spectra from the FDTD model without conductor losses from [7], along with predictions for thick gold and lead filters using the FDTD model with conductor losses, are shown in Fig. 11. These results illustrate that the measured losses of the filters are consistently higher than the simulated data. The listed discrepancies will be discussed in Section V.

It is also possible to model these filters as equivalent lumped resonant circuits. Although the equivalent circuit is not derived from the filter geometry, but merely fitted to the measured data, it may account for the variations in insertion loss and Q-factor by making the equivalent-circuit resistance a function of the surface resistance of the filter. The equivalent circuit is shown in Fig. 12 along with lumped-element values obtained by curve fitting the spectra of the gold and lead filters (from Fig. 7) to

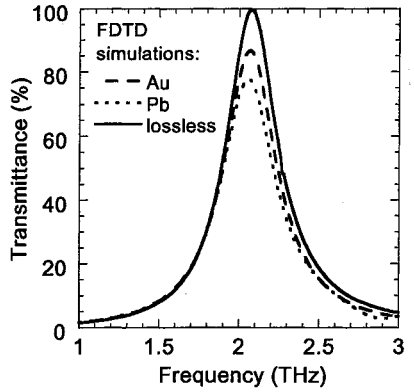

Fig. 11. FDTD model for thick gold (dashed line), lead (solid line), and lossless (solid line) films.

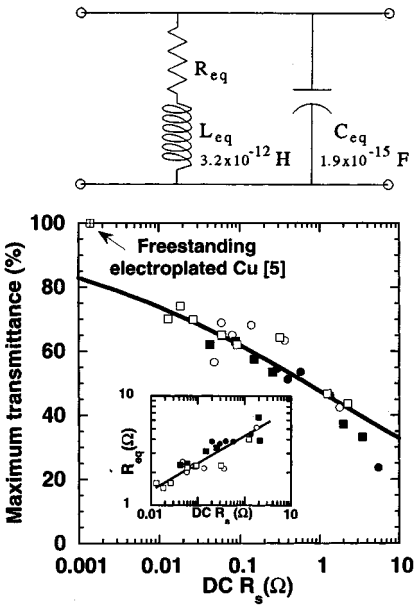

Fig. 12. (a) Lumped-element equivalent circuit with element values fitted to measured spectra (7). (b) Transmittance versus dc resistance of the films. The line through $R_{\rm eq}$ values is the approximation of (5). The measured transmittance of a bare polyester film 3.8-μm thick is 93%.

the following expression for the transmittance of the equivalent circuit:

$$T(\omega) = \frac{1}{\left[1 + \dfrac{R_{\rm eq} Z_0}{2\omega^2 L_{\rm eq}^2}\right]^2 + \left[\dfrac{Z_0\left(\dfrac{\omega}{\omega_0} - \dfrac{\omega_0}{\omega}\right)}{2\omega_0 L_{\rm eq}}\right]^2} \tag{5}$$

which has $L_{\rm eq}$ $R_{\rm eq}$, and ω_0 (and, therefore, $C_{\rm eq}$) as free parameters and $Z_0 = 377\text{s}\ \Omega$. As expected, only the equivalent-circuit resistance varies between the filters with different metal. The fitted values for $R_{\rm eq}$ can be approximated by the relation

$$R_{\rm eq} \approx 4.3 \cdot R_S^{0.25} \tag{6}$$

where R_S and $R_{\rm eq}$ are values for film thicknesses greater than the skin depth. A plot of the data from Fig. 7, along with the approximation obtained by substituting the above in (5), is shown

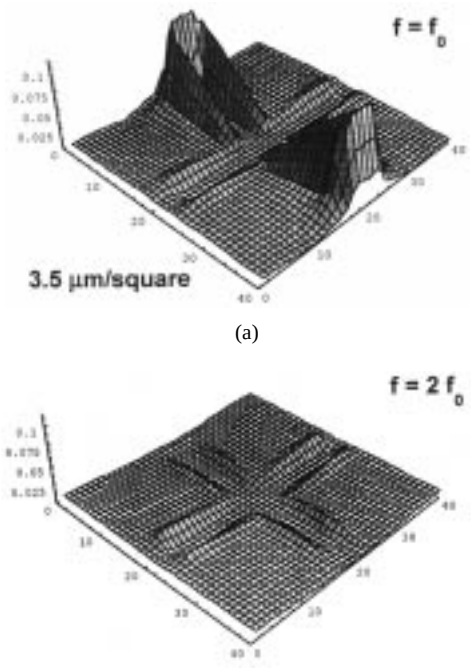

(a)

(b)

Fig. 13. (a) Current density magnitude at resonance and (b) twice the resonant frequency as calculated from a full-wave method-of-moments theory [16]. The plots show strong current peaks around the slot edges at resonance.

in Fig. 12. This reinforces the conclusion that the curve only extrapolates to approximately 85% transmittance for the calculated R_S of the filters from [5].

V. Discussion and Conclusions

In this paper, substrate-supported bandpass grid filters with adequate behavior at terahertz frequencies are demonstrated. The main advantage of the filters is ease of fabrication. The shift in resonant frequency caused by various substrate thicknesses can be accurately predicted by a FDTD technique, which also predicts some of the conductor loss. At oblique incidence, the filter performance shows some degradation, but is still acceptable for focused beams with large f numbers.

The insertion loss in the passband is found to scale with the product of metal conductivity and film thickness, i.e. with the dc surface conductance. The scaling was identical for lead and gold films for all thicknesses, including several classical skin depths. The observed variation in insertion loss with temperature indicates that geometrical effects, such as variations between the filters due to fabrication, are not a cause of the loss. The stopband attenuation increases with the metal film thickness until the classical skin depth is exceeded, and then, as expected, remains constant for thicker films. Therefore, the measured insertion loss and Q-factor dependence on the surface resistance shows that the effect of finite metal conductivity impacts the resonant and nonresonant properties in different ways. A possible explanation is that the evaporated metal films exhibit microstructural defects and grain boundaries [15] due to the low substrate temperature during deposition or due to flexing of the soft polyester substrate after deposition. Annealing the films to remove microstructural defects is not possible since the polyester substrates do not tolerate high temperatures.

The variation of insertion loss and Q-factor with the thickness of the metal film even when $t \gg \delta$ may arise from the resonant nature of the filters. The currents surrounding the slots have been simulated using a full-wave method-of-moments technique applied to a unit cell in an infinite grid [16], and are shown in Fig. 13. These currents peak at the ends of the slots at resonance, and this is likely to make the grid performance at resonance more sensitive to microstructural defects than in the stopband. This is even more pronounced at the slot edges, where additional effects, such as tearing of the film during liftoff or shadowing by the photoresist during deposition, may occur.

When extrapolating these results to films as thick as those of the electroplated freestanding filters in [5], a low loss, as demonstrated in [5], is not obtained, which indicates that evaporated metal grids may have limited transmittance as compared to the freestanding filters in [4] and [5], in which the metal has bulk properties. However, the fabrication process described here requires only a few hours and standard lithographic equipment, which is much easier and less costly than the fabrication of freestanding electroplated filters.

References

[1] T. K. Wu, Ed., *Frequency Selective Surface and Grid Array*. New York: Wiley, 1995.
[2] R. Urlich, "Interference filters for the far-infrared," *Appl. Opt.*, vol. 7, no. 10, pp. 1987–1996, Oct. 1968.
[3] P. Tomaselli, D. C. Edewaard, P. Gillan, and K. D. Moller, "Far-infrared bandpass filters from cross-shaped grids," *Appl. Opt.*, vol. 20, no. 8, pp. 1361–1366, Apr. 1981.
[4] M. Rebbert, P. Isaacson, J. Fischer, M. A. Greenhouse, J. Grossman, M. Peckerar, and H. A. Smith, "Microstructure technology for fabrication of metal-mesh grids," *Appl. Opt.*, vol. 33, no. 7, pp. 1286–1292, 1994.
[5] D. W. Porterfield, J. L. Hesler, R. Densing, E. R. Mueller, T. W. Crowe, and R. M. Weikle, II, *Appl. Opt.*, vol. 33, no. 25, pp. 6046–6052, Sept. 1994.
[6] R. J. Luebers and B. A. Munk, "Some effects of dielectric loading on periodic slot arrays," *IEEE Trans. Antennas Propagat.*, vol. 26, no. 4, pp. 536–542, July 1978.
[7] A. Alexanian, N. J. Colias, R. C. Compton, and R. A. York, "Three-dimensional FDTD analysis of quasi-optical arrays using Floquet boundary conditions and Beringer's PML," *IEEE Microwave Guided Wave Lett.*, vol. 6, pp. 138–140, Mar. 1996.
[8] S. T. Chase and R. D. Joseph, "Resonant array bandpass filters for the far-infrared," *Appl. Opt.*, vol. 22, no. 11, pp. 1775–1779, June 1983.
[9] M. E. MacDonald and E. N. Grossman, "Far-infrared bandpass filters," *SPIE Proc.–Int. Soc. Opt. Eng.*, vol. 2842, pp. 501–512, Aug. 1996.
[10] P. Callaghan, E. A. Parker, and R. J. Langley, "Influence of supporting dielectric layers on the transmission properties of frequency selective surfaces," *Proc. Inst. Elect. Eng.*, pt. H, vol. 138, no. 5, pp. 448–454, Oct. 1991.
[11] D. B. Rutledge, D. P. Neikerk, and D. P. Kasilingam, "Integrated circuit antennas," in *Infrared and Millimeter Waves*, K. J. Button, Ed. New York: Academic, 1983, vol. 10.
[12] R. C. Compton, R. C. McPhedran, G. H. Derrick, and L. C. Botten, "Diffraction properties of bandpass filters," *Infrared Phys.*, vol. 23, no. 5, pp. 239–245, 1983.
[13] S. M. Sze, Ed., *Physics of Semiconductor Devices*, 2nd ed. New York: Wiley, 1981.
[14] S. Ramo, J. R. Whinnery, and T. Van Duzer, Eds., *Fields and Waves in Communication Electronics*. New York: Wiley, 1984.
[15] T. J. Couts, Ed., *Electrical Conduction in Thin Metal Films*. Amsterdam, The Netherlands: Elsevier, 1974.
[16] S. C. Bundy and Z. B. Popović, "A generalized analysis for grid oscillator design," *IEEE Trans. Microwave Theory Tech.*, vol. 42, pp. 2486–2491, Dec. 1994.

Michael E. MacDonald (S'83–M'85) was born in Waltham, MA, in 1961. He received the B.S. degree in electrical engineering from Northeastern University, Boston, MA, in 1985, and the Ph.D. degree in electrical engineering from the University of Colorado at Boulder, in 1996. His doctoral work was conducted at the National Institute of Standards and Technology under the PREP Fellowship Program.

Since 1996, he has been a staff member at the Massachusetts Institute of Technology (MIT) Lincoln Laboratory, Lexington, MA. His work involves the design and development of infrared and millimeter-wave instruments for remote sensing of the atmosphere from space.

Angelos Alexanian, photograph and biography not available at time of publication.

Robert A. York (S'85–M'89–SM'99) received the B.S. degree in electrical engineering from the University of New Hampshire, Durham, in 1987, and the M.S. and Ph.D. degrees in electrical engineering from Cornell University, Ithaca, NY, in 1989 and 1991, respectively.

He is currently an Associate Professor of electrical and computer engineering at the University of California at Santa Barbara (UCSB). His group at UCSB is currently involved with the design and fabrication of novel microwave and millimeter-wave circuits, microwave photonics, high-power microwave and millimeter-wave modules using spatial combining and wide-bandgap semiconductor devices, and application of ferroelectric materials to microwave and millimeter-wave circuits and systems.

Dr. York received the 1993 Army Research Office Young Investigator Award and the 1996 Office of Naval Research Young Investigator Award.

Zoya Popović (S'86–M'90–SM'99) received the Dipl.Ing. degree from the University of Belgrade, Serbia, Yugoslavia, in 1985, and the M.S. and Ph.D. degrees from the California Institute of Technology, Pasadena, in 1986 and 1990, respectively.

She is currently an Associate Professor of electrical and computer engineering at the University of Colorado at Boulder. Her research interests include microwave and millimeter-wave quasi-optical techniques and active antenna arrays, high-efficiency microwave circuits, RF photonics, and antennas and receivers for radioastronomy.

Dr. Popović is a recipient of the 1993 URSI Young Investigator Award and the 1993 NSF Presidential Faculty Fellow Award, and the 1996 URSI International Issac Koga Gold Medal. She was also the recipient of the 1993 IEEE Microwave Theory and Techniques Society (IEEE MTT-S) Microwave Prize for pioneering work in quasi-optical grid oscillators.

Erich N. Grossman received the A.B. degree from Harvard University, Cambridge, MA, in 1980, and the Ph.D. degree from the California Institute of Technology, Pasadena, in 1987, both in physics. His doctoral dissertation involved the construction and testing of an ultra-low-noise far-infrared heterodyne receiver for airborne astronomy using cryogenic Ge:Ga photomixers.

From 1988 to 1989, he was a Post-Doctoral Fellow at the University of Texas at Austin, working jointly in the Astronomy and Electrical Engineering Departments. In 1989, he joined the National Institute of Standards and Technology (NIST), Boulder, CO, where he is currently a Project Leader for the High-Performance Sensors, Detectors, and Mixers Project. He is involved in the field of infrared and submillimeter device physics. His notable accomplishments at NIST include the development and experimental demonstration of the world's highest frequency high-efficiency lithographic antennas, and of the world's highest frequency Josephson junctions.

Dr. Grossman was the recipient of a 1993 Department of Commerce Gold Medal.